On the Molecular Mechanism of Water Reorientation

Damien Laage*,†,‡ and James T. Hynes†,‡,§

Chemistry Department, Ecole Normale Supérieure, 24 rue Lhomond 75005 Paris, France, CNRS UMR Pasteur, and Department of Chemistry and Biochemistry, University of Colorado, Boulder, Colorado 80309-0215

Received: June 13, 2008; Revised Manuscript Received: September 4, 2008

We detail and considerably extend the analysis recently presented in *Science* 2006, *311*, 832−835 of the molecular mechanism of water reorientation based on molecular dynamics simulations and the analytic framework of the extended jump model (EJM). The water reorientation is shown to occur through large-amplitude angular jumps due to the exchange of hydrogen (H)-bond acceptors, with a minor contribution from the diffusive H-bond frame reorientation between these exchanges. The robust character of this mechanism with respect to different water models is discussed. We fully characterize these jump events, including the distributions of trajectories around the average path. The average path values and the distributions of the jump time and the jump amplitude, the two key parameters in the Ivanov jump model component of the EJM, are determined. We also discuss the possibility of selectively exciting water molecules close to the jump event, of interest for ultrafast infrared experiments. In addition to a comparison of predicted reorientation times with experimental results, the reorientation time temperature dependence is discussed. A detailed description of the pathway free energetics for the water reorientation is presented; this is used to identify the jump rate-limiting step as the translational motion in which the initial H-bond of the reorientating water is elongated and the new H-bond acceptor water approaches.

1. Introduction

Many of liquid water's special and ubiquitous properties originate from its propensity to form very dynamic, labile hydrogen (H)-bond networks.[1−5] A major fashion in which this network constantly rearranges by breaking and forming H-bonds is through the reorientation of water molecules. This rearrangement also occurs when the water hydration pattern adapts to a changing solute, and water reorientation is at the heart of hydration dynamics. Thus, for chemical processes involving a charge redistribution in aqueous solution, a major response of the water solvent is the reorientation of individual water molecules. Examples in aqueous solution include S_N2 reactions[6] and proton transfer,[7,8] where the reaction coordinate for the latter involves water reorientation.[7,8] Similarly, the reaction coordinate governing proton transport[9−11] both in bulk water or in water wires within biological channels such as in gramicidin A involves the reorientation of water molecules; this is possibly the rate-limiting step,[10,12] but a detailed description remains elusive.[11] Water reorientation also determines the hydration layer lability around biological macromolecules such as proteins or DNA strands and thus conditions the biomolecule flexibility and function, such as the selective molecular recognition of ligands.[2,13,14]

Several mechanisms describing the molecular reorientation of water have been suggested over the years. One such is the "flickering clusters" mechanism,[1] relying on the concept of cooperative H-bonds; when an H-bond disappears, an entire water cluster dissolves, allowing the water molecules to reorient before forming a new H-bond. Another suggestion is based on an analogy with the reorientation mechanism in ice,[1,15] involving the diffusion of Bjerrum orientational defects. However, notwithstanding occasional concerns about the degree of its validity,[1,2,16−19] by far the most widely employed mechanism to describe water reorientation is the Debye small-step diffusion model.[20]

We have recently argued that the diffusive model is inadequate and that, instead, water reorientation proceeds mainly through large-amplitude angular jumps involving H-bond partner exchange for the reorienting water molecule.[21] Indeed, the reorientation was described in terms of a chemical reaction involving the exchange of H-bond partners for the reorienting water.[21] In the present paper, we detail and significantly extend this previous work, aspects of which are emphasized in the following description of the remainder of this paper.

We present in section 2 the molecular jump mechanism. We first very briefly review the shortcomings of the diffusive model and then extend our previous description based on an average path to include distributions of the jump angle and the waiting time for the jump. The distribution of the OH frequency and the probability to selectively excite a system close to the jump event, of interest in ultrafast infrared experiments, are also presented. Further, the sensitivity of the primary results to H-bond definitions and water potential is discussed. Section 3 turns to the detailed discussion of the analytic extended jump model, including an improved description of the model jump time. Calculated reorientation times at room temperature are compared with experimental results. In section 4, we provide for the first time a discussion of the reorientation time temperature dependence, a detailed description of the pathway free energetics for the water reorientation, and an identification of the rate-limiting step in the process. Section 5 provides some concluding remarks.

* To whom correspondence should be addressed. E-mail: damien.laage@ens.fr.
† Ecole Normale Supérieure.
‡ CNRS UMR Pasteur.
§ University of Colorado.

10.1021/jp805217u CCC: $40.75
Published on Web 10/23/2008

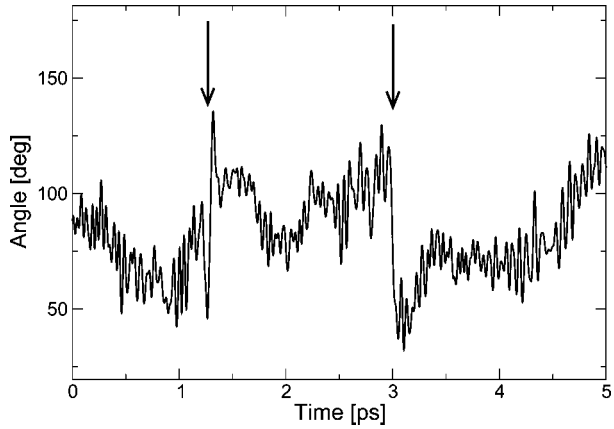

Figure 1. Time evolution of the angles between a selected OH-bond and a laboratory frame axis. The arrows indicate the presence of large-amplitude jumps.

2. Molecular Jump Mechanism

2.1. The Shortcomings of the Diffusive Model. We first briefly review the Debye diffusive model widely employed to describe water reorientation. It describes the reorientation as an angular Brownian motion, that is, a sequence of uncorrelated "infinitely small", or, more physically stated, very small amplitude, angular steps. Such an overdamped rotational Brownian motion picture[20] is not a priori implausible if one considers that a water molecule is in more or less continuous strong interaction with its neighbors via hydrogen bonds. A more detailed image for its justification for its applicability is that water first has to break at least one H-bond to reorient; the resulting dangling OH then performs a random search for a new H-bond acceptor, during which it reorients.

However, inspection of trajectory results for the time-dependent orientation of individual water O−H bonds shows the occurrence of sudden large-amplitude angular jumps (see Figure 1), incompatible with the very small amplitude assumption.

Examination of reorientation time values reveals another difficulty with the diffusive model more closely connected to experiment. Within the diffusive model, the orientational correlation functions

$$C_n(t) = \langle P_n[\mathbf{u}(0)\cdot\mathbf{u}(t)]\rangle \tag{1}$$

where P_n is the nth-rank Legendre polynomial and $\mathbf{u}$ a vector attached to the molecule, each follows a monoexponential decay whose time constants are the reorientation times τ_n, determined by the rotational diffusion constant D_R[22]

$$\tau_n = \frac{1}{n(n+1)D_R} \tag{2}$$

The ratio of the first two orientational relaxation times should therefore be $\tau_1/\tau_2 = 3$. This ratio is not directly measurable experimentally (vide infra) but can be obtained from molecular dynamics (MD) simulations (Table 1). The numerical ratio is only 2.0, thus departing clearly from the ideal diffusive value. The discrepancy is more pronounced for the τ_1/τ_3 ratio, which is predicted to be exactly 6 from the diffusive model and which is 3.1 in the MD simulations.

A further and more striking problem appears when one attempts to calculate the τ_n reorientation times directly from the rotational diffusion constant D_R. Assuming a diffusive reorientation mechanism, D_R can be calculated via MD simulations through the angular mean square displacement $\langle\theta^2(t)\rangle$ (see, for example, ref 23)

$$D_R = \lim_{t\to\infty} \frac{1}{4t}\langle\theta^2(t)\rangle \tag{3}$$

The averaged isotropic rotational diffusion coefficient D_R has been estimated from simulations[24] to be $D_R = 0.39$ ps^{-1} for water at 298 K, leading to an approximate τ_2 value of 0.4 ps, which is dramatically shorter, by about a factor of from five to seven, than the estimates from both simulations and experiments (see Table 1). It should also be noted that eq 3 should be used with extreme care. Indeed, as shown in Appendix B, the validity conditions of eq 3 are much more stringent than those for the translational counterpart.

All of these difficulties clearly show that the diffusive model is unable to describe the reorientational dynamics in water. We have indeed recently argued that water reorientation rather proceeds mainly via large angular jumps occurring during an exchange of H-bond acceptors plus a slower, less important, component related to the H-bond axis diffusive reorientation.[21] We now recall the main features of this extended jump model (EJM) and characterize it further.

2.2. Jump Reorientation: H-Bond Exchange. Here, we expand the discussion of ref 21 describing the elucidation of the jump mechanism of the water reorientation. New features include a more than 25-fold increase of the number of trajectories examined, an improved procedure for the selection of successful jumps based on the Stable States Picture of reactions, the presentation of distributions to augment the characterization beyond the average mechanistic path, and commentary on the sensitivity of the results to the use of different potentials and different definitions of the H-bond.

Since in the mechanism of ref 21 the angular jumps of a water O*H* bond are a consequence of the trading of H-bond acceptors receiving a H-bond from this water O*H*, these events have to be characterized, and a set of criteria defining the existence of a H-bond needs to be chosen. A wide variety of H-bond criteria have been suggested (see, for example, ref 25), based either on geometric conditions, energetic considerations, or orbital occupancy. We have adopted a widely employed geometric definition based on two distances and an angle, $R_{OO} < 3.5$ Å, $\theta_{HOO} < 30°$, $R_{OH} < 2.45$ Å (see Figure 2). We have verified that all of the results below are unchanged, both qualitatively and quantitatively, when another H-bond definition is adopted, such as, for example, the one recently suggested in ref 25 and based on the σ^*_{OH} orbital occupancy (see section 3.1).

We a posteriori analyze a MD trajectory and record all of the times a water O*H* that was initially H-bonded to a water oxygen O^a becomes H-bonded to a different oxygen O^b. For each of these switch events, we examine the sequence preceding it and the sequence following it, as long as no other H-bond exchange occurs. The time evolution of several key quantities is calculated along each exchange trajectory. More than 414000 H-bond exchanges are so collected, and the choice of a common time origin when the O*H* vector lies on the $\widehat{O^aO^*O^b}$ bisector plane allows the calculation of an average trajectory and of the distributions around it.

We first describe the average path for the switch event, which should provide a useful charaterization, before analyzing the spread of individual trajectories around it. This mean path starts

TABLE 1: Reorientation Times Obtained Respectively from Our MD Simulations, The Diffusive Model, The Simple Jump Model, The Frame Reorientation between the Jumps, the EJM, and the Experiments[a]

	τ_D (ps)	τ_1 (ps)	τ_2 (ps)	τ_2^{int} (ps)	τ_3 (ps)	τ_1/τ_2	τ_1/τ_3
MD (SPC-E)	9.7[b]	4.9	2.5	1.7	1.6	2.0	3.1
OH diffusion ($D_{OH} = 0.45$ ps^{-1})		1.1	0.4		0.2	3.0	6.0
jump model ($\Delta\theta = 68°$, $\tau_0 = 3.3$ ps)		8.1	3.6		2.7	2.4	3.4
OO frame reorientation		15.5	5.6		2.9	2.8	5.4
extended jump model (eq 7)		5.3	2.2[c]		1.4	2.4	3.6
experiment	8.5[d]	2−7.5[e]	1.9−3.0[f]	1.7−2.6[g]			

[a] τ_D is the Debye relaxation time and τ_2^{int} is the time integral of the C_2 tcf, relevant in NMR. [b] Ref 18. [c] See ref 85. [d] Ref 75. [e] Refs 2, 110, and 111. [f] Refs 80, 81, and 112. [g] Refs 71−74.

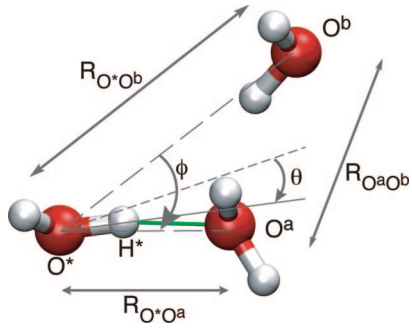

Figure 2. Definition of the different geometric coordinates employed to describe the H-bond exchange event; $R_{O^*O^a}$, $R_{O^*O^b}$, and $R_{O^aO^b}$ are the distances between the different water molecules, θ is the angle between the O*H* bond and the bisector plane of $\widehat{O^aO^*O^b}$, and ϕ is the $\widehat{O^aO^*O^b}$ angle.

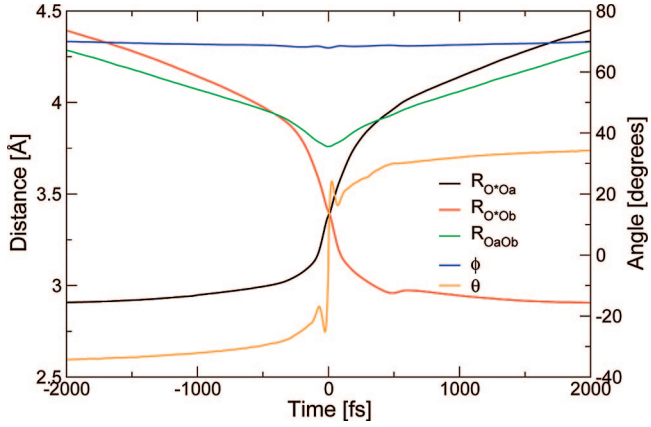

Figure 3. Average H-bond exchange trajectory: time-evolution of the geometric coordinates defined in Figure 2. The time origin $t = 0$ is defined by $\theta = 0$.

with O* H-bonded to the initial acceptor O^a, while the future partner O^b lies in the second shell of O* (Figure 3). The number of H-bonds received by the three oxygens O*, O^a, and O^b are equal to the bulk equilibrium values, that is, $\langle n_{O^*}\rangle = \langle n_{O^a}\rangle = \langle n_{O^b}\rangle \simeq 1.8$ (Figure 4). Following some fluctuations in the water H-bond network, possibly involving other previous remote angular jumps, O^a becomes overcoordinated while O^b becomes undercoordinated (Figure 4). This facilitates the motion of O*−H* away from the overcoordinated initial acceptor O^a and toward the undercoordinated final partner O^b. The details of the mechanism free energetics are presented in section 4.

Although during this H-bond exchange/reorientation event only H-bonds rather than covalent bonds are broken and formed, we consider it useful to regard it as a chemical reaction.[21] Indeed, by analogy with the proton coordinate in proton-transfer reactions, the O*−H* bond orientation (described by the θ angular coordinate defined in Figure 2) can be considered as a fast coordinate responding nearly adiabatically to the reorganization of the slower environment. This environment includes, for example, the H-bond lengths and is the actual reaction coordinate, as will be further elaborated in section 4. Such rearrangement of the environment before a chemical step can occur seems to be common to many processes in condensed phases, such as proton transfer[7,8] and proton transport in acidic[9,10] and basic[26] solutions or even in protein−protein recognition.[27,28]

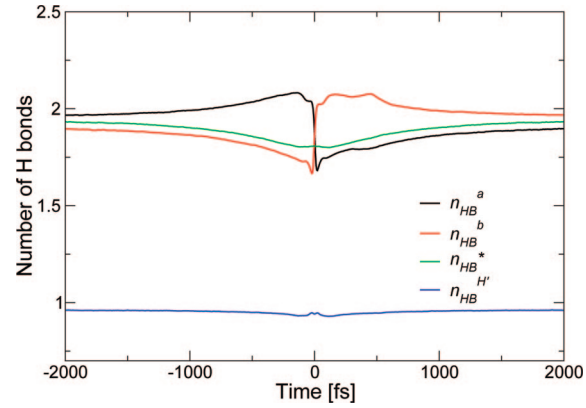

Figure 4. Average H-bond exchange trajectory: time-evolution of the H-bond coordination numbers. The $n_{HB}^{a,b,*}$ are the number of H-bonds received by O^a, O^b, and O*, respectively, and $n_{HB}^{\{H'\}}$ is the number of H-bonds donated by O* via its other hydrogen besides H*.

The environment first rearranges (Figure 5a) to reach the symmetric configuration where O^a and O^b are equidistant from O*, thus providing two energetically equivalent H-bond acceptors for H* (Figure 5b).[29] The initial O*H*···O^a H-bond then breaks concertedly with the formation of the new O*H*···O^b H-bond, inducing an angular jump in the O*H* bond orientation. The transition-state (TS) structure (Figure 5c) for both the slow environment and fast angular coordinates therefore corresponds to a totally symmetric bifurcated H-bond configuration, where H* donates a H-bond to both O^a and O^b. The angular jump interchanges the overcoordination and undercoordination defects between O^a and O^b, respectively. These defects subsequently disappear through fluctuations of the solution H-bond network. The reorientation process ends with the departure of O^a from the O* first shell since they are no longer H-bonded (compare panels c and d of Figure 5) and the stabilization of O^b in the O* first shell due to the new H-bond (Figure 3). The average jump amplitude is estimated to be 68° from the angle between the initial O*H*···O^a and final O*H*···O^b H-bond axes in the TS geometry when the jump occurs (Figure 3).

The reorientation mechanism is therefore concerted, and reorientation and H-bond breaking/forming occur simultaneously once the environment has reorganized. This provides a lower (free) energy path compared to the often suggested one where

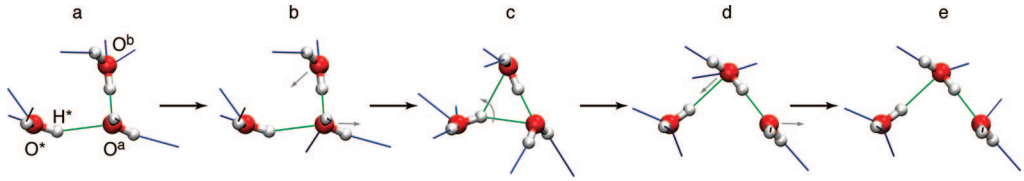

Figure 5. Five-step molecular mechanism for water reorientation.

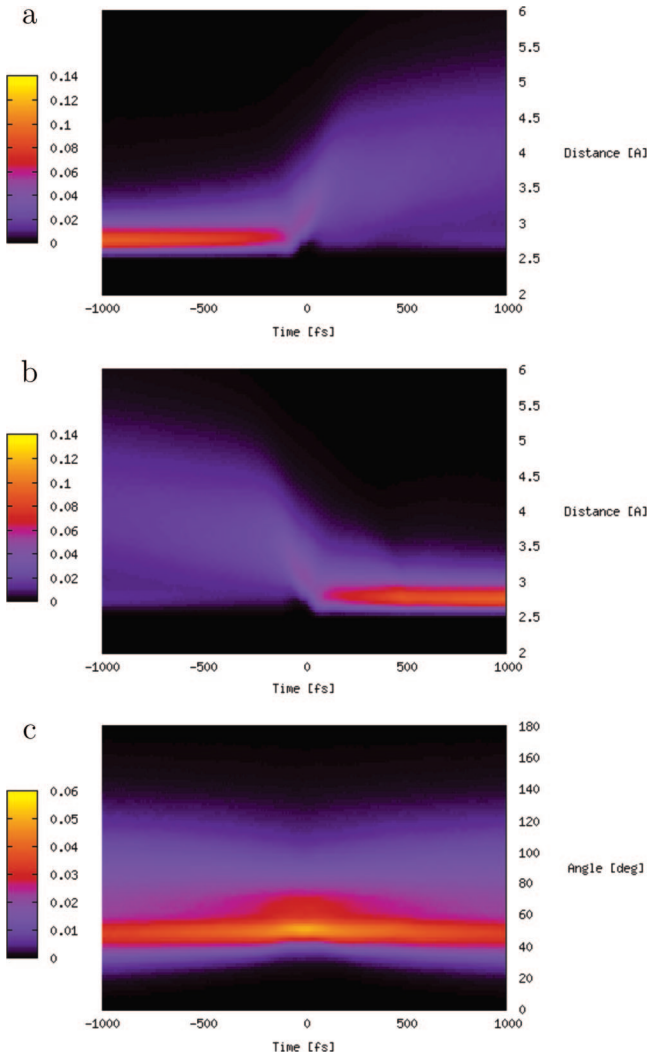

Figure 6. Distribution of coordinates versus time for successful H-bond exchange water reorientation trajectories: $R_{O^*O^a}$, $R_{O^*O^b}$, $\phi_{O^aO^*O^b}$.

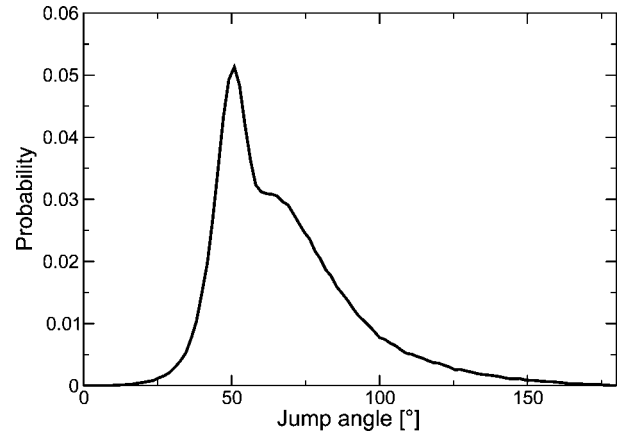

Figure 7. Jump angle distribution, determined as a cut in the distribution of $\phi_{O^aO^*O^b}$ values (Figure 6c) when the jump occurs at $t = 0$.

a water has to first fully break a H-bond before reorienting.[2] Here, a new H-bond is formed at the same time that the old one is lost.[30]

We now turn to the study of the successful trajectories distribution around the average pathway described above. Figure 6a shows the distribution of $R_{O^*O^a}$ distances before and after the jump event. This distribution reflects the conditions employed to collect the trajectories. O* and O^a are initially H-bonded through H*, and while transient H-bond breakings are allowed, H* should not form a H-bond with any other partner; therefore, for $t < 0$, the $R_{O^*O^a}$ distribution is narrow and limited by the geometric H-bond condition ($R_{O^*O^a} < 3.5$ Å). After the H-bond partner exchange, there is no longer any restriction on $R_{O^*O^a}$; most frequently, the former acceptor leaves the O* first shell because there is no longer any H-bond attracting it to O*, and subsequently, it diffuses away. However, in some cases, O^a forms back a H-bond with O* through its other hydrogen (not H*). Figure 6b shows the distribution of $R_{O^*O^b}$ distances, which is the symmetric reflection of the $R_{O^*O^a}$ distribution. In Figure 6c, the distribution of $\widehat{O^aO^*O^b}$ initial and final acceptors is seen to be quite narrow and might therefore be adequately represented by the average displayed in Figure 3. We pursue this further since this angle is especially important when the jump occurs where it provides the jump angular amplitude, and a cut of the distribution at $t = 0$ is provided in Figure 7. This distribution of jump angles is characterized by its average value of 68°, its standard deviation of 23°, and its skewness parameter 1.2.[31] The distribution is peaked at around 50° and is not symmetric; it displays a longer tail toward larger jump amplitudes, while there are practically no jumps occurring with amplitudes below 40°. This is due to steric hindrance between the initial and final water partners, and this angle corresponds to the $\widehat{O^aO^*O^b}$ angle when in the symmetric TS configuration the O^a and O^b waters are at their minimum approach distance, ≃2.5 Å as given by the O−O radial distribution function; this is an additional confirmation that the diffusive model, involving a sequence of very small angular jumps, does not apply.

Further improvements of our model should use these distributions rather than the average values. However, we first develop here a simple description based on the average H-bond exchange path, which will prove below to satisfactorily describe the experimental results.

It has been implied[32] that the observed angular jumps might be artifacts of the simple rigid nonpolarizable SPC/E[33] model that we have employed. While work[34−38] subsequent to our initial effort[21] has supported the jump picture, we have nonetheless repeated our study with two different water force fields, the rigid nonpolarizable TIP5P-E[39] model and the state-of-the-art polarizable and flexible Amoeba[40] force field. These calculations lead to the same picture for water reorientation, with only some minor differences in the reorientation times (see Table 2). Refining the description of the electronic structure with first-principles MD, such as, for example, a Car−Parrinello[41] scheme,

TABLE 2: Comparison of the Reorientation Times Respectively Obtained from the Three-Site Nonpolarizable Rigid SPC-E Model,[33] the Five-Site Nonpolarizable Rigid TIP5P-E[39] Model, and the Polarizable and Flexible Amoeba[40] Model

force field	τ_1 (ps)	τ_2 (ps)	τ_3 (ps)	τ_1/τ_2	τ_1/τ_3	τ_0 (ps)	$\Delta\theta$ (°)	τ_2^{frame}	τ_2^{extjump} (ps)
SPC-E	4.9	2.5	1.6	2.0	3.1	3.3	68	5.6	2.2
TIP5P-E	4.8	2.5	1.8	1.9	2.7	3.0	72	7.7	2.2
Amoeba	6.6	3.5	2.6	1.9	2.5	3.8	68	10.1	2.9

is of interest but is not expected to lead to any improvement. Indeed, the H-bond exchange process involves neither the breaking nor forming of covalent bonds and does not lead to any significant electronic structure rearrangements; therefore, the classical MD description should be sufficient.[42] Another possible improvement is the inclusion of a quantum treatment of the hydrogen vibrations, and very recently, such simulations have confirmed the nondiffusive jump reorientation behavior of liquid water.[35]

2.3. The Jump Mechanism and OH Stretching. A natural question is whether the jump mechanism implies that the water reorientation might be accelerated for weakly H-bonded waters, with a blue-shifted O*−H* stretch frequency of ω_{OH}.[43] The evolution of this frequency ω_{OH} along the average pathway has already been presented in ref 43. The frequency calculation is detailed in ref 43, and we do not repeat it here. We extend this analysis to the distribution of frequencies shown in Figure 9. While the average frequency is markedly blue shifted at the transition state, the probability distribution far from the transition state is quite broad along ω_{OH}, and the probability on the blue side is non-negligible. Hence, exciting water molecules on the blue edge of the absorption band will not specifically select water molecules close to the transition state, even though their fraction in the selected ensemble will be larger than that for frequencies in the center of the band. This is exemplified more quantitatively by the plot in Figure 8 of the probability to be within a 125 fs delay (close to the duration of the large-amplitude reorientation) of the transition state for different ω_{OH} values; for example, even for the most blue-shifted frequencies, only approximately 20% of the selected systems are within 125 fs of the transition state. It is seen, for example, that even for the most blue-shifted frequencies, the probability to be close to the transition state is still small;[44] indeed, the H-bond breaking is not the rate-limiting step in the H-bond exchange process, as will be shown below in section 4.2 and as we have argued previously.[43]

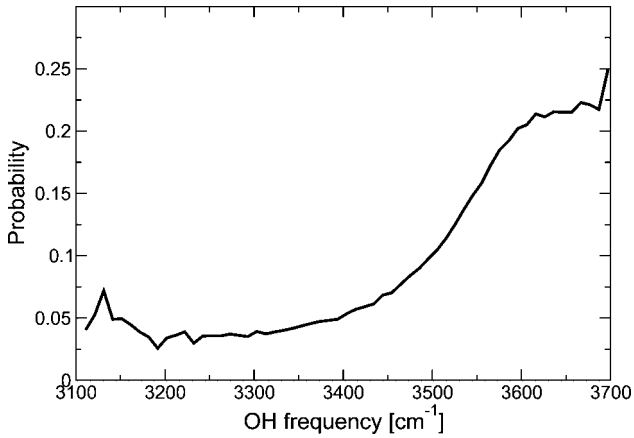

Figure 8. Probability to be within 125 fs of the transition-state structure for different ω_{OH} values.

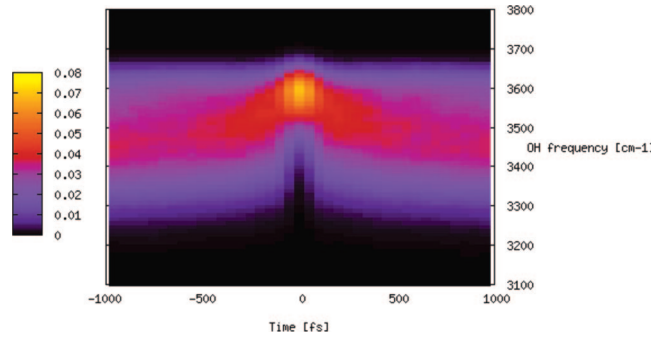

Figure 9. Average OH frequency ω_{OH} along the average reorienting H-bond exchange path, together with the distribution.

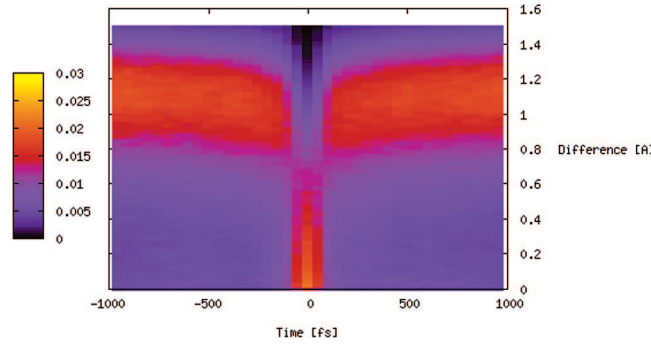

Figure 10. Distribution of ΔR_H along the average reorienting water H-bond exchange path.

Following our initial work,[21,43] several authors have confirmed that the reaction coordinate for the H-bond exchange is not simply the H-bond breaking, which can be monitored by the OH frequency.[34,45] These authors have made the interesting suggestion that the difference ΔR_H of the distances between the exchanging H* and the two closest oxygens (except O*) could be used as a reaction coordinate. We believe that defining the reaction coordinate through the OO distances and the angular coordinate as described above leads to a more instructive picture, distinguishing between the slow and fast coordinates. Nonetheless, the distribution of ΔR_H displayed in Figure 10 is evidence that this coordinate discriminates the transition state much better than does the OH frequency (Figure 9). Unfortunately, monitoring the ΔR_H coordinate appears not to be currently experimentally feasible. The contribution of various coordinates to the evolving reaction coordinate will be further discussed in section 4.2.

2.4. Contrast with Other Mechanisms. The water reorientation mechanism found here and in ref 21 contrasts with the mechanisms which have been previously suggested. From a MD simulation study of supercooled water, Sciortino et al.[46] have suggested that five-coordinated defects play a key role in transitions between different water structures. In the present mechanism however, we find that the five-coordinated, bifurcated H-bond configuration is an unstable transition state and is not a stable intermediate structure with a faster reorientation rate, as in ref 46. The jump reorientation mechanism that we find in liquid water differs also from the mechanisms found in small water clusters or in ice. In clusters,[47] the mechanism proceeds through a transition-state structure which minimizes the energy cost associated with H-bond breaking, as in the liquid, but the many dangling OHs in the cluster provide many more degrees of freedom to the reorienting waters than in the bulk where the waters are H-bonded to their neighbors, and the reorientation mechanisms are significantly different. Indeed, the cluster mechanism[47] involves the motion of a water OH whose

H is never at any point involved in H-bonding. In water ice,[15] the transition-state structure for the jumps of Bjerrum L defects is similar to the that one we find in the liquid with a bifurcated H-bond configuration; however, due to the high rigidity of the ice network, the exchange between the first and second shells observed in the liquid is hindered and is replaced by a limited lattice distortion.[48]

Several studies[49,50] have also addressed the mechanism of H-bond breaking in water, which occurs through an angular motion in liquid water. However, this is a different issue than the one studied here, which is the H-bond exchange, that is, the formation of a new, distinct, stable H-bond. These works could not discriminate between transient H-bond breakings leading to an unstable dangling OH from H-bond breakings concerted with a H-bond formation with a new partner; the majority of H-bond breaking events are due to large-amplitude librations, without any H-bond exchange (in section 3.1, the H-bond lifetime is shown to be much shorter than the H-bond exchange time). In addition, ref 49 considered as a final state a broken H-bond configuration, which is not a stable state, in contrast to the present study which describes the path between two stable states; ref 50 also considered as an intermediate state a situation where the initial H-bond is broken but the initial partner remains in the first shell, which is shown here to be unstable. The coupling between rotation and translation of a H-bond acceptor in liquid water had also been studied;[51] this differs from the present work where we consider the rotation of a H-bond donor, but the picture provided in ref 51 should apply to the motion of the O^a departing water in our mechanism.

3. Reorientation Times

Here, we expand the discussion of ref 21 describing the determination of the reorientation times within an extended jump model. The new features include a new procedure for the calculation of the jump time, that is, the inverse jump rate constant, based on the Stable States Picture[52,53] of reactions, which leads to a more robust estimate of the jump time and which is consistent with the average jump mechanism determination procedure described above, and the comparison of the jump time with the various definitions of the hydrogen-bond lifetime. An explicit treatment of the librational reorientation is also added.

3.1. Jump Model. The experimental signature of the large-amplitude (≃68°) angular jumps of a water molecule is to be expected in the orientational time correlation functions (tcfs) and the associated reorientation times. The orientational relaxation times due to the angular jumps can be determined through the jump model developed by Ivanov.[54]

The Ivanov model is an extension of the diffusive angular Brownian motion picture to finite amplitude jumps. It assumes that the jumps have a constant amplitude, are uncorrelated, and occur with a frequency of $1/\tau_0$. In this simple model, the jump directions are supposed to be isotropic, which is reasonable for water where the OH rotational diffusion constant is close to the average isotropic rotational diffusion constant.[18,24,55] The jump model has been generalized to anisotropic jump distributions,[56−58] but as just mentioned, the isotropic description is expected to be sufficient and has the advantage of simplicity. Another model approximation is that angular jumps are instantaneous; we will see below that this is reasonable for water, where the jump time is approximately 10 times shorter than the average time interval between jumps. A final approximation is that the water OH bond directions remain fixed between jumps. This last assumption is in fact not valid for water and will be removed in section 3.2.

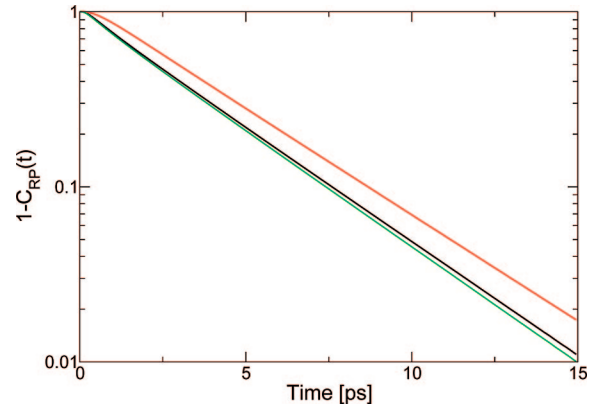

Figure 11. Time correlation function $1 - C_{RP}(t)$, whose relaxation time is the jump time τ_0. The correlation function is shown for different H-bond (HB) existence criteria; in black is a first set of geometric conditions ($R_{OO} < 3.1$ Å, $R_{HO} < 2.0$ Å, $\theta_{HOO} < 20°$), in red is another set with stricter geometric conditions ($R_{OO} < 2.9$ Å, $R_{HO} < 1.8$ Å, $\theta_{HOO} < 10°$), and in green is the HB definition of ref 25 with a minimum occupancy of the σ^*_{OH} orbital of 0.015 (stricter than the 0.0085 minimum value suggested in ref 25 for the existence of HB). The respective relaxation times are 3.3, 3.5, and 3.3 ps for the three sets of conditions.

We first detail the reorientation times associated with the angular jumps due to the H-bond exchanges. Within the Ivanov model, the τ_n relaxation times are[54]

$$\tau_n^{\text{jump}} = \tau_0\left\{1 - \frac{1}{2n+1}\frac{\sin[(n+1/2)\Delta\theta]}{\sin(\Delta\theta/2)}\right\}^{-1} \qquad (4)$$

where τ_0 is the jump time and $\Delta\theta$ is the angular jump amplitude.[59] These two parameters can be obtained from our MD simulations, as now explained.

The $\Delta\theta$ jump amplitude cannot be directly obtained by comparing the O*H* orientations before and after the H-bond exchange because of the non-negligible amplitude of the librational motions of a water molecule. We therefore consider the angle between the initial average O*H* direction, that is, the $O^*H^*\cdots O^a$ H-bond axis, and the final direction, that is, the $O^*H^*\cdots O^b$ H-bond axis; this is therefore the $\widehat{O^aO^*O^b}$ angle when the jump occurs. The average value of this jump angle was determined above to be $\Delta\theta \simeq 68°$.

In our description,[21] the τ_0 jump time is the inverse rate constant for the H-bond exchange event, an activated process which we treat as a chemical reaction. Rearrangements of the water H-bond network are known to occur on a picosecond time scale,[2−4] indicating that the reaction barrier is low—a few times the thermal energy k_BT—and is thus frequently sampled by the system. With such a lower barrier, however, one anticipates that each excursion close to the transition-state (TS) barrier top need not lead to a successful reaction and thus that recrossing effects on the rate constant can be large[60] (see section 4.3 where the transmission coefficient is estimated to be $\kappa \simeq 0.5$ at 300 K). These unsuccessful reorientation attempts only lead to a transient, unstable reorientation and do not contribute to the long-time reorientation. These failed jump attempts appear as large-amplitude librations, whose contribution to the reorientation is fast but limited, as detailed in section 3.4. To determine the long-time reorientation, only the successful, stable jumps should be considered; for that, and to improve our original

methodology in ref 21, we employ the Stable States Picture (SSP),[52,53] which relies on the definition of stable reactant (R) and product (P) states instead of defining the TS dividing surface.

The stability requirement for R and P can be imposed either via a minimum lifetime condition or via H-bond criteria more strict than that normally employed (see section 2.2). We have verified that these two possibilities lead to equivalent results, and we present here only those obtained via the latter route. We note that we have also studied the influence of the type of H-bond definition, for example, geometric, energetic, or based on orbital occupancy. While we have found that a TS reactive flux approach[61] is very sensitive to the details of the H-bond definition, we have verified that this is not the case with the SSP; we have employed tight geometric H-bond conditions (R_{OO} < 3.1 Å, R_{HO} < 2.0 Å, θ_{HOO} < 20°), and Figure 11 shows that the results are very similar to those obtained with stricter criteria or with another recently suggested H-bond definition based on the σ^*_{OH} orbital occupancy.[25]

In the SSP approach, we calculate the exchange rate constant, and thus the H-bond exchange or jump time, from the cross correlation function

$$C_{RP}(t) = \langle n_R(0) n_P(t) \rangle \quad (5)$$

where $n_{R,P}(t)$ is the probability for the system to be in the stable R and P states, respectively, and which gives the probability to have formed a stable product at time t when the system was in the reactant at time 0. We employ absorbing boundary conditions in the product to avoid spurious effects from subsequent H-bond exchanges from the first-formed product. The decay time of the complementary probability then provides the desired jump time τ_0: $1 - C_{RP}(t) = \exp(-t/\tau_0)$. The results shown in Figure 11 give the time as $\tau_0 = 3.3$ ps. Because the H-bond exchange in water induces a departure of the initial partner, the jump time is related to the water residence time.[62,63]

We pause to compare this H-bond exchange time τ_0 to two other time scales which have been suggested to describe the H-bond network dynamics, namely, the continuous and intermittent H-bond lifetimes, τ_{HB}^{cont} and τ_{HB}^{int}.[64−67] The τ_{HB}^{cont} lifetime corresponds to the time during which a H-bond exists continuously without any interruption, while τ_{HB}^{int} is the H-bond survival time, irrespective of any transient breaking. The H-bond exchange time just calculated should certainly be longer than τ_{HB}^{cont} because many H-bond breakings occur, and the old H-bond is re-formed, without the presence of a new H-bond acceptor. We expect that, in contrast, the H-bond exchange time should be shorter than τ_{HB}^{int}. This follows from the feature that after a H-bond exchange and the formation of a new stable H-bond, another H-bond exchange can occur, leading back to the initial H-bond partner; τ_{HB}^{int} is therefore longer than the exchange time. From our simulations, we confirm that the H-bond exchange time $\tau_0 = 3.3$ ps (Figure 11) is indeed longer than $\tau_{HB}^{cont} = 0.5$ ps[67] and shorter than $\tau_{HB}^{int} = 6.5$ ps.[67]

Finally, we have also investigated the Markovian nature of the H-bond exchanges. Figure 12 shows the distribution of waiting times before the jump obtained from the collection of successful jump events. The distribution is not Poissonian for short waiting times, which shows that there is a memory effect at short delays. However, for time scales longer than approximately 2 ps, the distribution follows an exponential decay whose characteristic time is the SSP jump time τ_0.

3.2. Frame Reorientation. As shown in ref 21 and mentioned in section 3.1, the simple jump model needs to be complemented to reach a full description of water reorientation in solution due to the failure of the Ivanov jump model assumption that the orientation remains fixed between jumps. For water, this would imply that as long as an O*H*···O H-bond remains intact, the O*H* direction remains frozen. This is of course not the case for two reasons; the O*H* bond librates around the O*H*···O H-bond axis, and the latter axis itself slowly rotates.[21] Librations occur on a subpicosecond time scale and do not affect the long-time reorientation decay; their treatment is detailed in section 3.4. In contrast, the slower reorientation of the H-bond axis between the jumps must be accounted for in an extended jump model (EJM).

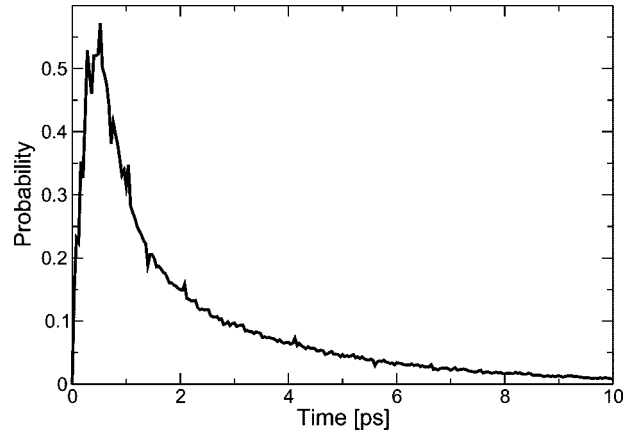

Figure 12. Distribution of waiting times before a successful water angular jump event.

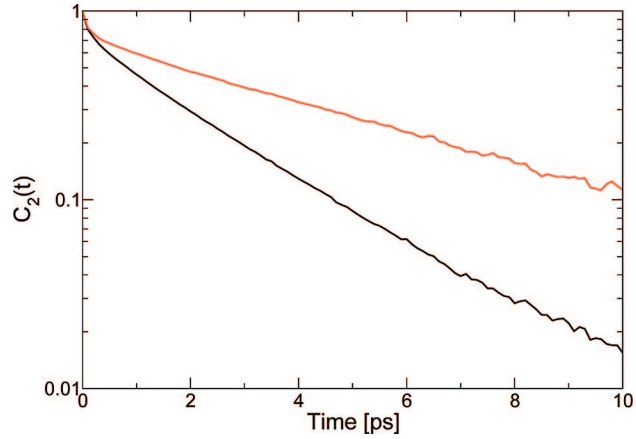

Figure 13. Water (second Legendre polynomial) orientational time correlation function: full reorientation (black) and reorientation between jumps (red) at 300 K.

The H-bond axis reorientation is determined from the MD simulations by calculating the $C_n(t)$ orientational correlation functions (eq 1) between two successive H-bond switches (Figure 13). In liquid water, this frame reorientation component τ_n^{frame} is slower than the jump component τ_n^{jump}, as seen in Figure 13 and Table 1.

In strong contrast with the OH reorientation, the H-bond axis reorientation between H-bond switches follows a diffusive behavior. This is shown by the individual trajectories which do not exhibit any large-amplitude angular jumps even when the OH direction displays such jumps, as seen in Figure 14 and its contrast with Figure 1. In addition, the axis reorientation times ratios (Table 1) are very close to the ideal diffusive values.

3.3. Extended Jump Model. The jump and frame reorientation components can be combined within an EJM to describe the reorientation time past the initial fast but limited librational

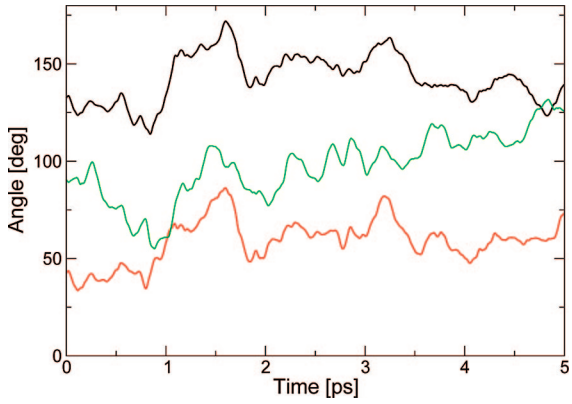

Figure 14. Time evolution of the angles between a selected OH···O H-bond axis and the three *x*, *y*, and *z* laboratory frame axes, respectively. The same OH as that in Figure 1 was selected, together with the oxygen which accepts a H-bond from it between 1.2 and 3 ps. Note the absence of angular jumps, in contrast to the OH orientation shown in Figure 1.

reorientation.[21] The jump and frame motions are independent because the occurrence of jumps depends on the approach of a new H-bond partner while the frame reorientation does not; the resulting orientational tcf is therefore the product of the two tcfs (see ref 68 on the consequence upon reorientation of decoupled internal and overall motions, which is widely employed in NMR, either for proteins[69] or for polymers[70]). Thus, we write

$$C_n(t) = \langle P_n[\mathbf{u}_{OH}(0)\cdot\mathbf{u}_{OH}(t)]\rangle = \langle P_n[\tilde{\mathbf{u}}_{OH}(0)\cdot\tilde{\mathbf{u}}_{OH}(t)]\rangle \times \langle P_n[\mathbf{u}_{OO}(0)\cdot u_{OO}(t)]\rangle \quad (6)$$

where $\mathbf{u}_{OH}$ is the OH orientation in the laboratory frame, $\tilde{\mathbf{u}}_{OH}$ is the OH orientation in the local OO frame, and $\mathbf{u}_{OO}$ is the OO H-bond axis orientation in the laboratory frame. The tcfs $C_n(t)$ are thus a product of two exponential decays, giving the overall reorientation time τ_n as the EJM equation

$$\frac{1}{\tau_n} = \frac{1}{\tau_n^{jump}} + \frac{1}{\tau_n^{frame}} \quad (7)$$

This description is sufficient to treat the longer-time reorientation time behavior.[21] For some purposes however, such as dealing with the fully time-integrated tcfs measured by NMR,[71−74] inclusion of shorter time scale contributions is required, as now discussed.

3.4. Short-Time Librational Reorientation. Librational motions also induce an OH reorientation. However, their characteristic time scale is subpicoseconds, and they only lead to limited reorientation within an angular cone centered on the H-bond axis. As detailed, for example, in refs 36 and 43, they can be effectively modeled by an exponential decay, such that the resulting complete orientational tcf is

$$C_n(t) = [(1 - C_{lib})e^{-t/\tau_n^{lib}} + C_{lib}]e^{-t[(1/\tau_n^{jump})+(1/\tau_n^{frame})]} \quad (8)$$

where τ_n^{lib} is an effective subpicosecond time and C_{lib} is related to the librational cone semiangle α by

$$C_{lib} = \left[\frac{1}{2}\cos(\alpha)\,(1 + \cos(\alpha))\right]^2 \quad (9)$$

3.5. Resulting Reorientation Times. Table 1 summarizes the different values obtained for the orientational relaxation times. These values are taken from experiments when available, from our MD simulations, from the diffusive model, from the jump model using the jump amplitude $\Delta\theta$ and jump time τ_0 values determined from the simulations, from the OO frame rotational relaxation between H-bond exchanges, and from the EJM combining jump and frame reorientation. Before proceeding with a detailed discussion, we need to consider some aspects of the experimental times.

The first-order relaxation time τ_1 is not directly accessible experimentally. It can be inferred from the experimental Debye dielectric relaxation time τ_D,[75,76] but the latter describes collective motions, and the connection to the single-molecule τ_1 time involves several approximations depending on the choice of dielectric relaxation theory used to make the collective to single-molecule conversion. The resulting range of possible τ_1 values is therefore very wide.

Regarding the second-order time τ_2, experimental determinations are available from several sources, NMR,[55,77−79] femtosecond infrared spectroscopy,[80,81] and quasi-elastic neutron scattering (QENS).[82] The time resolution of ultrafast infrared spectroscopy allows the determination of the $C_2(t)$ tcf, from which a fit of the long-time component yields τ_2. In contrast, the longer time scale NMR spectroscopy measures only the time-integrated $C_2(t)$;[83] because of the initial librational decay (see section 3.4), this integrated time is shorter than (in our description) the extended jump relaxation time τ_2. We therefore provide in Table 1 both the τ_2 long-time fit and the τ_2^{int} time-integrated values from the simulations. The EJM leads to the long-time value, and the time-integrated result can be obtained if needed, with some additional information on the initial librational decay (see section 3.4).[84]

Table 1 shows first that the MD simulations are fully consistent with the available experimental relaxation times, thus confirming the validity of our methodology. We now turn to model results. First, the comparison of the reorientation times predicted by the diffusive model with the experimental and simulation results shows very poor agreement. The ratio of the successive MD reorientation times, such as, for example, τ_1/τ_2, departs noticeably from the ideal diffusive values; the values predicted by the diffusive model for the reorientation times themselves differ by a factor of 4 or more. Second, for the EJM, the predicted reorientation times are in good agreement with both the experiments and the simulation results.[85] The departure of the reorientation time ratios from the diffusive values is also properly reproduced. Finally, we note that while the inclusion of the frame reorientation component within the EJM shortens the reorientation times compared to the simple jump model predictions, the main reorientation component remains the angular jump.

4. Temperature Dependence, Energetics, and Free Energetics

In this section, we turn our attention to the temperature dependence of the τ_2 reorientation time and its associated activation energy. We then discuss the free-energy profile for the reorientation and the contributions to the activation free energy. This discussion also provides insight on the evolving character of the reaction coordinate for the reorientation.

4.1. Temperature Dependence and Activation Energies. In order to examine the title topic, we have repeated our analysis at different temperatures between 285 and 373 K from simulations run with the SPC-E model at the experimental density[86]

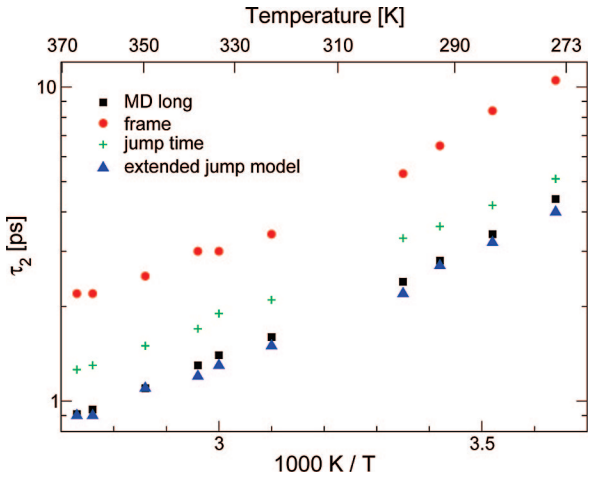

Figure 15. Temperature dependence of the water τ_2 reorientation time and its components: tcf long-time decay from the simulations, frame component τ_2^{frame}, jump time τ_0, and resulting EJM time τ_2^{extjump}.

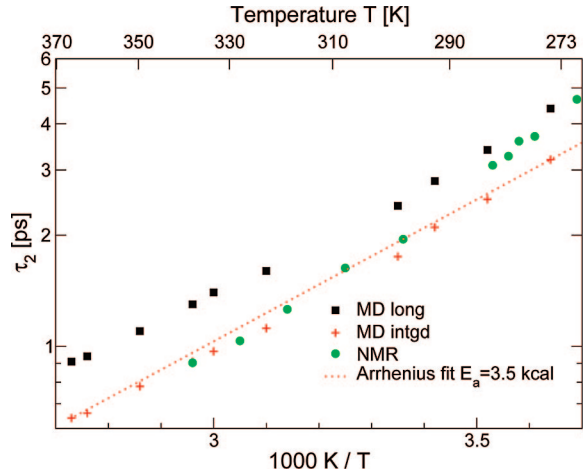

Figure 16. Temperature dependence of the water τ_2 reorientation time determined from the long-time component of the reorientational decay in the simulations, from the integrated reorientation time, and from NMR experiments,[74] together with an Arrhenius fit with a 3.5 kcal/mol activation energy.

under atmospheric pressure (see Appendix A for the methodological details). We focus on the τ_2 reorientation time, for which extensive NMR results are available.[74]

We first demonstrate, in Figure 15, that the EJM adequately describes the MD simulation (long) reorientation time throughout the temperature range. This figure also displays the temperature dependence of the two components, those of the distinct jump and frame reorientation processes, of the EJM reorientation time. The activation energies for these two contributions appear to be similar (which is remarkable given their distinctly different character), indicating that both processes contribute to reorientation at all temperatures in the range examined, with the jump contribution always remaining the more important.

Figure 16 shows the τ_2 reorientation times obtained from NMR experiments[74] and from our MD simulations, with both the long-time fit of $C_2(t)$ and its time integral, which is the quantity to be compared with NMR values. The agreement between our simulations and the experiments is fairly good. For temperatures lower than 285 K, the agreement deteriorates, probably due to the very low fusion temperature of SPC-E water (215 K[87]). Several types of temperature dependences have been suggested for the water reorientation times, such as exponential (Arrhenius-like),[75,82] fractional power law,[19,88−90] and Vogel−Tammann−Fulcher,[89] and this topic is still a matter of debate. An Arrhenius fit of the MD τ_2 times on the entire temperature range (Figure 16) leads to a 3.5 kcal/mol activation energy, consistent with the 3.1 kcal/mol value obtained from fsIR spectroscopy[91] for the center of the ω_{OH} band and somewhat larger than the 1.85 kcal/mol inferred from QENS experiments.[82] This is also in good agreement with the 3.1 kcal/mol activation energy obtained by an Arrhenius fit of dielectric relaxation measurements on the 315−367 K temperature range.[75,92]

4.2. Free-Energy Profile. Finally, we examine the free energetics of the reorientation process, whose mechanism was described in section 2.2. We determine the free-energy evolution along the average reaction path and study its different contributions.

For this purpose, we return to the reference temperature of 300 K and generate a free-energy surface as a function of the three reduced coordinates, $\Delta n_{HB} = n^a_{HB} - n^b_{HB}$, $\Delta R = R_{O^*O^a} - R_{O^*O^b}$, and θ, describing, respectively, the changes in the initial and final acceptor H-bond coordination numbers, the changes in the distances from the rotating water to the initial and final acceptors, and the angular coordinate (see Appendix A). The free energy G is calculated from the probability distribution p determined via the MD simulations as

$$G(\Delta n_{HB}, \Delta R, \theta) = -k_B T \ln[p(\Delta n_{HB}, \Delta R, \theta)] \quad (10)$$

Instead of propagating a trajectory on this free-energy surface, which is quite rugged, we use the average jump trajectory determined in section 2.2 (see Figures 3 and 4). We then obtain the free-energy profile along the reaction path. The contributions coming from each coordinate are known at each point along the trajectory from a differential approach

$$dG = \frac{\partial G}{\partial \Delta n_{HB}} d\Delta n_{HB} + \frac{\partial G}{\partial \Delta R} d\Delta R + \frac{\partial G}{\partial \theta} d\theta = dG_{\Delta n_{HB}} + dG_{\Delta R} + dG_\theta \quad (11)$$

and are integrated along the reaction path from the reactant to the transition state

$$\Delta G_i^{\ddagger} = \int_R^{\ddagger} dG_i \frac{di}{ds} ds \quad (12)$$

where $i = \Delta n_{HB}, \Delta R, \theta$. Symmetry is employed to generate the subsequent free-energy behavior. The results are displayed in Figure 17.

The total free-energy barrier in Figure 17 is approximately $\Delta G^{\ddagger} \simeq 2.0 \pm 0.1$ kcal/mol. This is noticeably smaller than the E_a Arrhenius activation energy determined above (section 4.1) because of the temperature dependence of the rate constant prefactor, as will be detailed in section 4.3.

We now focus on the comparison between the different contributions to the free-energy barrier, which will provide further insight on the evolving nature of the reaction coordinate for the water reorientation. It is evident from Figure 17 that the highest free-energy barrier contributor, and thus the rate-limiting step in the jump mechanism, is the asymmetric translational motion of the departing old partner and that of the incoming new acceptor (see the mechanistic Figure 5). In contrast, and perhaps initially surprisingly, the changes in the H-bond

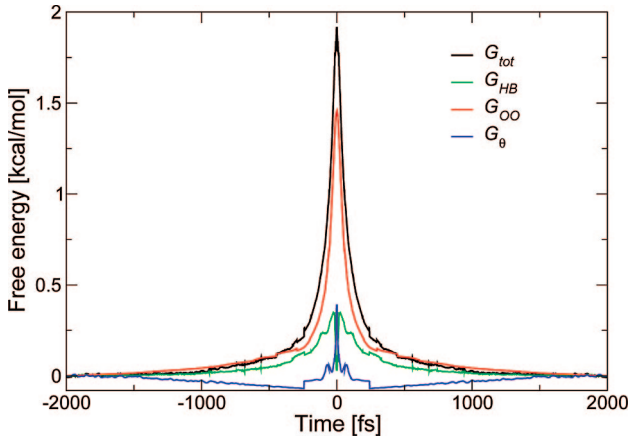

Figure 17. Free-energy profile along the reaction path and contributions from the different coordinates (symmetrized around $t = 0$).

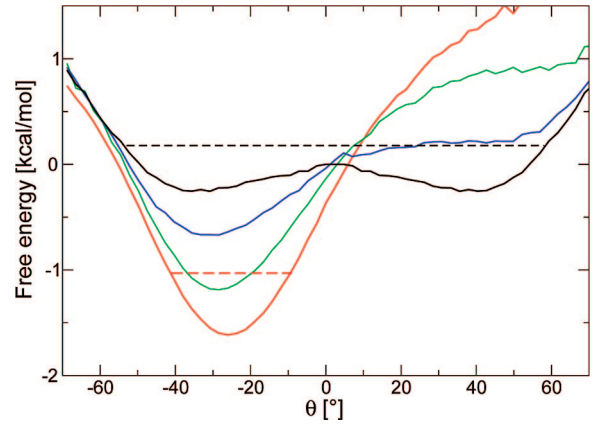

Figure 18. Cuts in the free-energy surface along the angular θ coordinate for $n_{HB}^{a} = n_{HB}^{b}$ and $R_{O^*O^a} - R_{O^*O^b}$ equal to, respectively, -1 (red), -0.5 (green), -0.2 (blue), and 0 Å (black). The global free-energy origin is arbitrarily taken at $R_{O^*O^a} - R_{O^*O^b} = 0$ and $\theta = 0$. The dashed lines represent the zero-point vibrational energy along θ for the reactant and transition states (see the text).

coordination numbers do not give a large contribution to the barrier. However, these changes are of relatively small amplitude (see Figure 4), such that they would relatively easily occur thermally.

The identification of the reorientation rate-limiting step as the translational motion in and out of the rotating water's hydration shell is in strong contrast with previous suggestions (see, for example, refs 2, 19, and 93) that it is the breaking of one of the rotating water's H-bonds. This points again to the concerted nature of the reorientation mechanism, where H-bond breaking and reorientation occur simultaneously once the environment has reorganized.

We pause to note that this concerted character has implications, for example, for the Grotthus mechanism of proton transport in water, where water reorientation was argued to be the rate-limiting step; the barrier is not simply due to the H-bond cleavage as has been suggested[10] but rather to the shell exchange.[94] The free-energy difference between a free dangling OH and a H-bonded OH[95] cannot therefore be used to evaluate the activation energy of the proton mobility as previously suggested[10] since a H-bond is never fully broken in the reorientation mechanism.

Several cuts in the free-energy surface along the rotating OH* θ coordinate for $\Delta n_{HB} = n_{HB}^{a} - n_{HB}^{b} = 0$ and different values of $\Delta R = R_{O^*O^a} - R_{O^*O^b}$ are shown in Figure 18. These cuts give a perspective on the reorientation process when the environmental coordinate of the initial and final acceptor H-bond coordination numbers has already reached its transition-state value. In the reactant configuration, $\Delta R < 0$, and there is a single free-energy minimum for O*H* H-bonded to O^a. No stable product with O*H* H-bonded to O^b can be formed since the environment has not yet reorganized. This is analogous to the situation for proton-transfer reactions,[8] where the fast proton coordinate (which is the analogue of the angle θ) adapts to the slow environment coordinate (here, the asymmetric translation ΔR). Once the environment has reached the transition-state configuration (here, $\Delta R = 0$), the free-energy profile along θ becomes a symmetric double well. This emphasizes that the crossing of the transition state by the angular motion is activated, as can be also seen in Figure 17, and that the bifurcated H-bond configuration shown in Figure 5 is a transition state, that is, a free-energy saddle point, and not a stable configuration as previously suggested.[46]

Because the OH* rotation is a high-frequency fast motion, a better description would be to treat it quantum mechanically, in a fashion similar to that for the proton coordinate for proton transfer.[8] The resulting ground vibrational levels along the θ coordinate for the reactant and transition-state configurations of the other coordinates are shown in Figure 18.[96] In the transition-state configuration, the vibrational level is above the barrier top (as in the proton adiabatic limit),[97] and no tunneling is necessary for the angular jump; this is consistent with the observation that the kinetic isotope effect for the reorientation time is weak,[81] although a full examination of this effect is left for the future.

TABLE 3: Temperature Dependence of the Free-Energy Barrier $\Delta G^{\ddagger}$ and That of the Transmission Coefficient κ

temperature (K)	$\Delta G^{\ddagger}$ (kcal/mol)	κ
275	2.1 ± 0.1	0.51 ± 0.01
300	2.0 ± 0.1	0.53 ± 0.01
350	2.1 ± 0.1	0.60 ± 0.01
370	2.2 ± 0.1	0.69 ± 0.01

As noted above, the free-energy barrier due to the asymmetric translational motion ΔR brings the main contribution to the total barrier $\Delta G^{\ddagger} = 2.0 \pm 0.1$ kcal/mol, and this contribution can be approximately estimated by splitting it into three pair terms, one for the increase in the O^*-O^a distance, one for contraction of the O^*-O^b distance, and the last one for the change in the O^a-O^b distance. These pair free-energy terms are determined from the potential of mean force along the O−O distance in water $w(R)$ and lead to

$$\Delta G^{\ddagger} \simeq w(R^{\ddagger}_{O^*O^a}) - w(R^{\text{reactant}}_{O^*O^a}) + w(R^{\ddagger}_{O^*O^b}) - w(R^{\text{reactant}}_{O^*O^b}) + w(R^{\ddagger}_{O^aO^b}) - w(R^{\text{reactant}}_{O^aO^b}) \quad (13)$$

This sum of the pair contributions is ≃1.3 kcal/mol, in good agreement with the translational contribution to $\Delta G^{\ddagger}$ of ≃1.4 kcal/mol (see Figure 17). Such an estimate provides an easy way of predicting how the total free-energy barrier for the H-bond exchange process changes for different solutes.

4.3. Transmission Coefficient. We noted above that there is a noticeable difference between the reorientation free-energy barrier height $\Delta G^{\ddagger} = 2.0$ kcal/mol and the activation energy $E_a = 3.5$ kcal/mol. The additional source of temperature dependence of the jump rate constant lies in the rate prefactor. The rate constant can be expressed as

$$k(T) = \frac{1}{\tau_0(T)} = \kappa(T) A \exp\left(-\frac{\Delta G^{\ddagger}}{RT}\right) \quad (14)$$

where $A \exp(-\Delta G^{\ddagger}/RT)$ is the Transition-State Theory rate constant (see Appendix C). The transmission coefficient or barrier recrossing factor κ is, in principle, temperature-dependent, and the Arrhenius activation energy is

$$E_a = RT^2 \frac{\partial \ln k}{\partial T} = \frac{RT^2}{\kappa}\frac{\partial \kappa}{\partial T} + \Delta G^{\ddagger} + T\frac{\partial \Delta G^{\ddagger}}{\partial T} \quad (15)$$

in which the temperature dependence of A is ignored (see Appendix C).

The free-energy barrier $\Delta G^{\ddagger}$ is determined at a few temperatures in the liquid range together with the recrossing factor (see Appendix A for the methodology). The results listed in Table 3 show that there is very little temperature dependence of $\Delta G^{\ddagger}$. In contrast, the transmission coefficient κ is apparently sensitive to the temperature with an estimated contribution to the Arrhenius activation energy of $(RT^2/\kappa)(\partial\kappa/\partial T) \simeq 0.6 \pm 0.1$ kcal/mol. The term due to the temperature dependence of $\Delta G^{\ddagger}$, $T\partial\Delta G^{\ddagger}/\partial T$, suffers from a high uncertainty because of the uncertainty on the $\Delta G^{\ddagger}$ values at different temperatures and is estimated to be 0.3 ± 0.6 kcal/mol. The resulting estimate for the Arrhenius activation energy would therefore be 2.9 ± 0.8 kcal/mol, in fair agreement with the 3.5 kcal/mol determination from the temperature dependence study in section 4.1.

5. Concluding Remarks

We have described in detail an extended jump mechanism for the reorientation of water in solution originally presented in ref 21. This mechanism involves the exchange of H-bond acceptors, which we analyze as a chemical reaction. It involves large-amplitude jumps, which contrast with the sequence of very small reorientations as assumed in the diffusive model often adopted. This mechanism is concerted; the reorientation occurs in parallel with the breaking and forming of H-bonds. We have shown that the rate-limiting step is the antisymmetric translational motion of arrival of a new partner and the departure of the previous partner and not the H-bond breaking as commonly assumed. The reorientation times resulting from the mechanism can be analytically described by an extended jump model (EJM).

This angular jump mechanism is consistent with the experimental data for reorientation times, including their temperature dependence, as well as with the molecular dynamics simulations presented. It has received recent additional support from femtosecond infrared measurements[34] and from simulations using a quantum description of the nuclear motions.[35] This new picture has strong implications for the interpretation of experimental results, for which the diffusion model has been systematically used in the past. As shown elsewhere,[98] the reinterpretation of neutron scattering experiments on water[82] using the EJM reconciles those results with the reorientation times determined through other techniques such as NMR or ultrafast spectroscopies and MD simulations.

This extended jump picture has already been shown to successfully describe the reorientational dynamics of water around a chloride ion[36] and hydrophobic solutes[99] and should prove insightful for the complex study of water dynamics around proteins and DNA. This work is under way.

Possible improvements to the extended jump model could include the consideration of the jump angle distribution (see Figure 7), that of the jump time distribution (see Figure 12), or that of the jump anisotropy (see section 3.1). However, as noted within, the simple version of the EJM already captures the key features of water reorientation, and including these refinements would preclude the use of the simple expressions detailed here. These refinements are left for future investigation.

Acknowledgment. This work was supported in part by NSF Grants CHE-0417570 and CHE-0750477.

Appendix A: Methodology

The molecular dynamics simulations are run with the DL_POLY package[100] and the rigid nonpolarizable SPC-E[33] force field. All simulations are run in the microcanonical ensemble, at the experimental density,[86] after an equilibration at constant temperature. The long-range Coulombic forces are treated by Ewald summation, and the time step is 1 fs. The 300 K trajectory is propagated with 500 water molecules for 2 ns. At other temperatures, the trajectories are 300 ps long, and the simulation boxes contain 256 water molecules. The free-energy surfaces are determined from 10 ns simulations with 256 molecules.

Some further studies on the force field dependence of the results were performed with the rigid nonpolarizable TIP4P[101] TIP5P-E[39] models and with the Amoeba[102] polarizable and flexible model as implemented in Tinker.[40]

We have also performed test calculations on a larger simulation box with 500 water molecules to confirm the absence of size dependence of our results.

The transmission coefficient κ discussed in section 4.3 is calculated by generating 20 different initial TS configurations, as defined by $|\Delta R| < 0.1$ Å, $|\theta| < 3°$, and $|\Delta n_{HB}| < 0.1$. From each of these configurations, 20 trajectories are propagated both forward and backward in time, with initial velocities randomly sampled from a Maxwell−Boltzmann distribution at the chosen temperature. The κ is then determined by counting the number of trajectories which connect the reactant and product wells.

Appendix B: Rotational Diffusion Constant

Within the diffusion model and for an orientation θ free to diffuse in the $]-\infty;+\infty[$ interval, the orientation θ obeys the diffusion equation

$$\frac{\partial P(\theta, t|\theta_0, t_0)}{\partial t} = D_R \nabla_\Omega^2 P(\theta, t|\theta_0, t_0) \quad (16)$$

where $P(\theta, t|\theta_0, t_0)$ is the conditional probability that the orientation at time t is θ, provided it was θ_0 at time t_0, and ∇_Ω^2 is the angular Laplacian operator. Using the Green theorem, the mean square angular displacement therefore follows as

$$\frac{\partial \langle \theta^2(t) \rangle}{\partial t} = D_R \int \mathrm{d}\theta P(\theta, t|0, 0) \nabla_\Omega^2 \theta^2 \quad (17)$$

The explicit angular Laplacian factor in eq 17 is

$$\nabla_\Omega^2 \theta^2 = 2\left(1 + \theta \frac{\cos\theta}{\sin\theta}\right) \quad (18)$$

If θ is close to $2n\pi$, and only if that condition is fulfilled, this can be approximated as

$$\nabla_{\Omega}^{2}\theta^{2} \simeq 4 \tag{19}$$

leading to the well-known expression for the mean square angular displacement

$$\langle\theta^{2}(t)\rangle \simeq 4D_{\mathrm{R}}t \tag{20}$$

However, the validity of this approximation is very limited. In an angular Brownian motion picture where the reorientation proceeds through a sequence of very small jumps, the time t should be both long enough to be after the onset of the diffusive regime, that is, after several infinitesimal jumps, and not too long in order to still fulfill the $\theta \simeq 0$ condition. These two conditions cannot be both satisfied for water since the elementary angular jump size is 68°.[103]

Appendix C: Transition-State Theory Rate Constant

On the three-dimensional free-energy surface $G(\Delta n_{\mathrm{HB}}, \Delta R, \theta)$, the Transition-State Theory rate constant can be expressed as[104−107]

$$k_{\mathrm{TST}} = \frac{\omega_{\parallel}^{\mathrm{R}}}{2\pi}\frac{\omega_{\perp 1}^{\mathrm{R}}\omega_{\perp 2}^{\mathrm{R}}}{\omega_{\perp 1}^{\ddagger}\omega_{\perp 2}^{\ddagger}}\exp\Big[-\frac{1}{RT}(G(\Delta n_{\mathrm{HB}}^{\ddagger}, \Delta R^{\ddagger}, \theta^{\ddagger}) - G(\Delta n_{\mathrm{HB}}^{\mathrm{R}}, \Delta R^{\mathrm{R}}, \theta^{\mathrm{R}}))\Big] \tag{21}$$

where $\omega_{\parallel}^{\mathrm{R}}$ is the frequency of the reaction coordinate in the reactant state, $\omega_{\perp 1,2}^{\mathrm{R},\ddagger}$ are the frequencies of the transverse coordinates in the reactant and transition states, respectively, and $(\Delta n_{\mathrm{HB}}^{\mathrm{R},\ddagger}, \Delta R^{\mathrm{R},\ddagger}, \theta^{\mathrm{R},\ddagger})$ are the reactant and transition-state coordinates on the three-dimensional free-energy surface.

The reactant reaction coordinate can be approximated as the Δn_{HB} coordinate (see Figure 4) and thus $\omega_{\parallel}^{\mathrm{R}} \simeq \omega_{\Delta n_{\mathrm{HB}}}^{\mathrm{R}}$; in the transition state, the reaction coordinate (see Figures 4, 17, and 18) is close to the θ angular coordinate.

A precise determination of the temperature dependence of the prefactor in eq 21 (labeled A in eq 14) would require a normal-mode analysis on the free-energy surface. This is beyond the range of the present study, and we assume the temperature dependence to be negligible, focusing on that of the transmission coefficient κ.

References and Notes

(1) Eisenberg, D.; Kauzmann, W. *The Structure and Properties of Water*; Oxford Clarendon Press: London, 1969.

(2) Bagchi, B. *Chem. Rev.* **2005**, *105*, 3197–3219.

(3) Ohmine, I.; Tanaka, H. *Chem. Rev.* **1993**, *93*, 2545–2566.

(4) Fecko, C. J.; Eaves, J. D.; Loparo, J. J.; Tokmakoff, A.; Geissler, P. L. *Science* **2003**, *301*, 1698–1702.

(5) Rey, R.; Møller, K. B.; Hynes, J. T. *J. Phys. Chem. A* **2002**, *106*, 11993–11996.

(6) Gertner, B. J.; Whitnell, R. M.; Wilson, K. R.; Hynes, J. T. *J. Am. Chem. Soc.* **1991**, *113*, 74–87.

(7) Ando, K.; Hynes, J. T. *J. Mol. Liq.* **1995**, *64*, 25–37.

(8) Ando, K.; Hynes, J. T. *J. Phys. Chem. B* **1997**, *101*, 10464–10478.

(9) Marx, D.; Tuckerman, M. E.; Hutter, J.; Parrinello, M. *Nature* **1999**, *397*, 601–604.

(10) Agmon, N. *Chem. Phys. Lett.* **1995**, *244*, 456–462.

(11) Cukierman, S. *Biochim. Biophys. Acta* **2006**, *1757*, 876–885.

(12) Pomès, R.; Roux, B. *Biophys. J.* **1996**, *71*, 19–39.

(13) Levy, Y.; Onuchic, J. N. *Annu. Rev. Biophys. Biomol. Struct.* **2006**, *35*, 389–415.

(14) Chaplin, M. *Nat. Rev. Mol. Cell Bio.* **2006**, *7*, 861–866.

(15) Podeszwa, R.; Buch, V. *Phys. Rev. Lett.* **1999**, *83*, 4570–4573.

(16) Rahman, A.; Stillinger, F. H. *J. Chem. Phys.* **1971**, *55*, 3336–3359.

(17) O'Reilly, D. E. *J. Chem. Phys.* **1974**, *60*, 1607–1618.

(18) van der Spoel, D.; van Maaren, P. J.; Berendsen, H. J. C. *J. Chem. Phys.* **1998**, *108*, 10220–10230.

(19) Winkler, K.; Lindner, J.; Börsing, H.; Vöhringer, P. *J. Chem. Phys.* **2000**, *113*, 4674–4682.

(20) Debye, P. *Polar Molecules*; The Chemical Catalog Company: New York, 1929.

(21) Laage, D.; Hynes, J. T. *Science* **2006**, *311*, 832–835.

(22) In the analysis of experiments, the Debye diffusional model is often combined via the Einstein relation between the diffusion constant and the friction constant and a hydrodynamic model for the friction constant to produce the Debye−Stokes−Einstein relation in which D_{R} is inversely proportional to the solvent viscosity. The relationship between the rotational friction and the viscosity is logically distinct from eq 2, as already noted by Debye.[20]

(23) Mazza, M. G.; Giovambattista, N.; Starr, F. W.; Stanley, H. E. *Phys. Rev. Lett.* **2006**, *96*, 057803.

(24) Svishchev, I. M.; Kusalik, P. G. *J. Phys. Chem.* **1994**, *98*, 728–733.

(25) Kumar, R.; Schmidt, J. R.; Skinner, J. L. *J. Chem. Phys.* **2007**, *126*, 204107.

(26) Tuckerman, M. E.; Marx, D.; Parrinello, M. *Nature* **2002**, *417*, 925–929.

(27) Lange, O.; Lakomek, N.; Farès, C.; Schröder, G.; Walter, K. F. A.; Becker, S.; Meiler, J.; Grubmüller, H.; Griesinger, C.; de Groot, B. L. *Science* **2008**, *320*, 1471–1475.

(28) Boehr, D.; Wright, P. *Science* **2008**, *320*, 1429–1430.

(29) The rearrangement of the environment also involves the orientation of the O^{b} water with respect to O*H*, which is initially random and evolves to the proper configuration to receive a H-bond from H*, where the two hydrogens on O^{b} point away from H*.

(30) We note that this mechanism evidences that in liquid water, large-amplitude rotations are coupled with translational motion since the reorientation involves an exchange of water molecules within the first shell of O*. The jump reorientation mechanism is therefore likely to be also intrinsically related to translational motion in water, a topic under investigation (Laage, D.; Møller, K. B.; Hynes, J. T. in progress).

(31) Abramowitz, M.; Stegun, I. A. *Handbook of Mathematical Functions with Formulas, Graphs, and Mathematical Tables*; Dover: New York, 1964.

(32) Ludwig, R. *ChemPhysChem* **2007**, *8*, 44–46.

(33) Berendsen, H. J. C.; Grigera, J. R.; Straatsma, T. P. *J. Phys. Chem.* **1987**, *91*, 6269–6271.

(34) Loparo, J. J.; Roberts, S. T.; Tokmakoff, A. *J. Chem. Phys.* **2006**, *125*, 194522.

(35) Paesani, F.; Iuchi, S.; Voth, G. A. *J. Chem. Phys.* **2007**, *127*, 074506.

(36) Laage, D.; Hynes, J. T. *Proc. Natl. Acad. Sci. U.S.A.* **2007**, *104*, 11167–11172.

(37) Harpham, M. R.; Levinger, N. E.; Ladanyi, B. M. *J. Phys. Chem. B* **2008**, *112*, 283–293.

(38) Park, S.; Fayer, M. D. *Proc. Natl. Acad. Sci. U.S.A.* **2007**, *104*, 16731–16738.

(39) Rick, S. W. *J. Chem. Phys.* **2004**, *120*, 6085–6093.

(40) Ponder, J. W. *TINKER: Software Tools for Molecular Design*, v 4.2; Washington University School of Medecine: Saint Louis, MO, 2004.

(41) Car, R.; Parrinello, M. *Phys. Rev. Lett.* **1985**, *55*, 2471–2474.

(42) In addition, first-principles MD techniques suffer from a high computational cost, limiting the trajectory length to a few tens of picoseconds with a simulation box of a few hundred atoms, which is not sufficient here, and the simple DFT functional employed in these simulations is well known to lead to overstructured water.[108]

(43) Laage, D.; Hynes, J. T. *Chem. Phys. Lett.* **2006**, *433*, 80–85.

(44) We stress that this moderate frequency dependence of the jump probability should have only a limited impact on the reorientation. Indeed, the higher jump probability applies only as long as the delay between the excitation pulse and the jump is shorter than the frequency decorrelation time of approximately <1.5 ps,[109] and at these short delays, the strong frequency dependence of the initial (<200 fs) librational reorientation is already present.[43]

(45) Garrett-Roe, S.; Hamm, P. *J. Chem. Phys.* **2008**, *128*, 104507.

(46) Sciortino, F.; Geiger, A.; Stanley, H. E. *Nature* **1991**, *354*, 218–221.

(47) Keutsch, F. N.; Saykally, R. J. *Proc. Natl. Acad. Sci. U.S.A.* **2001**, *98*, 10533–10540.

(48) The translocation of Bjerrum D defects involves a different mechanism[15] with no bifurcated H-bond in the transition-state structure.

(49) Csajka, F. S.; Chandler, D. *J. Chem. Phys.* **1998**, *109*, 1125–1133.

(50) Luzar, A. *Faraday Discuss.* **1996**, *103*, 29–40.

(51) Svishchev, I. M.; Kusalik, P. G. *Chem. Phys. Lett.* **1993**, *215*, 596–600.

(52) Northrup, S. H.; Hynes, J. T. *J. Chem. Phys.* **1980**, *73*, 2700–2714.

(53) Grote, R. F.; Hynes, J. T. *J. Chem. Phys.* **1980**, *73*, 2715–2732.
(54) Ivanov, E. N. *Sov. Phys. JETP* **1964**, *18*, 1041–1045.
(55) Ropp, J.; Lawrence, C.; Farrar, T. C.; Skinner, J. L. *J. Am. Chem. Soc.* **2001**, *123*, 8047–8052.
(56) Alessi, L.; Andreozzi, L.; Faetti, M.; Leporini, D. *J. Chem. Phys.* **2001**, *114*, 3631–3639.
(57) O'Reilly, D. E.; Petersen, E. M. *J. Chem. Phys.* **1971**, *55*, 2155–2163.
(58) Diezemann, G.; Sillescu, H. *J. Chem. Phys.* **1999**, *111*, 1126–1136.
(59) Our attention has been recently drawn to previous work by O'Reilly which had already suggested, in part motivated by certain unpublished trajectory results of Stillinger and Rahman, that water reorientation occurs through large-amplitude jumps and had used the Ivanov model to determine the reorientation time τ_2.[17] However, ref 17 assumes that the angular jumps are caused by hard-sphere collisions and that the free-energy barrier lies along the angular coordinate; this is in clear contrast with the H-bond-centered picture we describe here, where, as detailed in section 4.2, the rate-limiting step is the rearrangement of the environment. In addition, no frame reorientation between the jumps is considered in ref 17.
(60) Hynes, J. T. The Theory of Reactions in Solution. In *Theory of Chemical Reaction Dynamics*; Baer, M., Ed.; CRC Press: Boca Raton, FL, 1985; pp 171−234.
(61) Chandler, D. *Introduction to Modern Statistical Mechanics*; Oxford University Press: New York, 1987.
(62) Laage, D.; Hynes, J. T. *J. Phys. Chem. B* **2008**, *112*, 7697–7701.
(63) However, for H-bond exchange around solutes such as halide ions, the two times can differ[62] since a H-bond exchange can occur before the reorienting water has left the ion hydration shell.
(64) Rapaport, D. C. *Mol. Phys.* **1983**, *50*, 1151–1162.
(65) Luzar, A.; Chandler, D. *Nature* **1996**, *379*, 55–57.
(66) Luzar, A. *J. Chem. Phys.* **2000**, *113*, 10663–10675.
(67) Chandra, A. *Phys. Rev. Lett.* **2000**, *85*, 768–771.
(68) Szabo, A. *J. Chem. Phys.* **1984**, *81*, 150–167.
(69) Tjandra, N.; Szabo, A.; Bax, A. *J. Am. Chem. Soc.* **1996**, *118*, 6986–6991.
(70) Soutar, H. L.; Swanson, L. *Macromol.* **1994**, *27*, 4304–4311.
(71) Smith, D. W. G.; Powles, J. G. *Mol. Phys.* **1966**, *10*, 451–463.
(72) Lankhorst, D.; Schriever, J.; Leyte, J. C. *Ber. Bunsen-Ges. Phys. Chem.* **1982**, *86*, 215.
(73) van der Maarel, J. R. C.; Lankhorst, D.; de Bleijser, J.; Leyte, J. C. *Chem. Phys. Lett.* **1985**, *122*, 541–544.
(74) Ludwig, R.; Weinhold, F.; Farrar, T. C. *J. Chem. Phys.* **1995**, *103*, 6941.
(75) Rønne, C.; Thrane, L.; Östrand, P. O.; Wallqvist, A.; Mikkelsen, K. V.; Keiding, S. R. *J. Chem. Phys.* **1997**, *107*, 5319–5331.
(76) Rønne, C.; Östrand, P. O.; Keiding, S. R. *Phys. Rev. Lett.* **1999**, *82*, 2888–2891.
(77) Lang, E.; Lüdemann, H. D. *J. Chem. Phys.* **1977**, *67*, 718–723.
(78) Lang, E.; Lüdemann, H. D. *Ber. Bunsen-Ges. Phys. Chem.* **1980**, *84*, 462–470.
(79) Lang, E. W.; Lüdemann, H. D. *Ber. Bunsen-Ges. Phys. Chem.* **1981**, *85*, 603–611.
(80) Tan, H. S.; Piletic, I. R.; Fayer, M. D. *J. Chem. Phys.* **2005**, *122*, 174501.
(81) Rezus, Y. L. A.; Bakker, H. J. *J. Chem. Phys.* **2005**, *123*, 114502.
(82) Teixeira, J.; Bellissent-Funel, M. C.; Chen, S. H.; Dianoux, A. J. *Phys. Rev. A* **1985**, *31*, 1913–1917.
(83) Abragam, A. *The Principles of Nuclear Magnetism*; Clarendon: Oxford, UK, 1961.
(84) A direct experimental measurement of the τ_3 time has not been performed yet, but promising time-resolved hyper-Rayleigh scattering techniques should allow its determination for water in the near future (T. Buckup, private communication).
(85) If instead of using the average jump angle $\langle\Delta\theta\rangle$ to calculate the jump time $\tau_2^{\text{jump}}(\langle\Delta\theta\rangle)$ one uses the jump angle distribution to determine the average jump time $\langle\tau_2^{\text{jump}}\rangle$, the extended jump model time τ_2 increases to 2.4 ps, in closer agreement with the MD simulation value. The effective jump angle $\Delta\theta^{\text{eff}}$ defined as $\tau_2^{\text{jump}}(\Delta\theta^{\text{eff}}) = \langle\tau_2^{\text{jump}}\rangle$ is then close to 56°.
(86) Kell, G. S. *J. Chem. Eng. Data* **1975**, *20*, 97–105.
(87) Vega, C.; Sanz, E.; Abascal, J. L. F. *J. Chem. Phys.* **2005**, *122*, 114507.
(88) Speedy, R. J.; Angell, C. A. *J. Chem. Phys.* **1976**, 851–858.
(89) Lang, E. W.; Girlich, D.; Lüdemann, H. D.; Piculell, L.; Müller, D. *J. Chem. Phys.* **1990**, *93*, 4796–4803.
(90) Kumar, P.; Franzese, G.; Buldyrev, S. V.; Stanley, H. E. *Phys. Rev. E* **2006**, *73*, 041505.
(91) Nienhuys, H. K.; van Santen, R. A.; Bakker, H. J. *J. Chem. Phys.* **2000**, *112*, 8487–8494.
(92) The Debye relaxation time is approximately $\tau_D \simeq (3\epsilon_0)/(2\epsilon_0 + \epsilon_\infty)\tau_2$, where $\epsilon_{0,\infty}$ are the water static and optical dielectric constants, respectively; for water, the temperature dependence of ϵ_0 is weak,[1] and the temperature dependences of τ_D and τ_2 are therefore similar.
(93) Chen, S. H.; Teixeira, J. *Adv. Chem. Phys.* **1986**, *64*, 1–44.
(94) The measured 2−3 kcal/mol activation energy for the proton mobility in water[10] is compatible with the activation energy that we determine for water reorientation.
(95) Walrafen, G. E.; Fisher, M. R.; Hokmabadi, M. S.; Yang, W. H. *J. Chem. Phys.* **1986**, *85*, 6970–6982.
(96) The OH rotation quantization slightly alters the activation free energy from the classical approximation discussed in section 4.2; we ignore this in the present work.
(97) Kiefer, P. M.; Hynes, J. T. *J. Phys. Chem. A* **2003**, *107*, 9022–9039.
(98) Laage, D.; Hynes, J. T. To be submitted.
(99) Laage, D.; Stirnemann, G.; Hynes, J. T. To be submitted.
(100) Smith, W.; Forester, T. R. *J. Mol. Graph.* **1996**, *14*, 136–141.
(101) Jorgensen, W. L.; Chandrasekhar, J.; Madura, J. D. *J. Chem. Phys.* **1983**, *79*, 926–936.
(102) Ren, P. Y.; Ponder, J. W. *J. Phys. Chem. B* **2003**, *107*, 5933–5947.
(103) The special character of the angular versus translational diffusion model has, for example, been recognized in ref 23.
(104) Glasstone, S.; Laidler, K. J.; Eyring, H. *The Theory of Rate Processes*; McGraw-Hill: New York, 1941.
(105) Fonseca, T.; Kim, H. J.; Hynes, J. T. *J. Mol. Liq.* **1994**, *60*, 161–200.
(106) Laage, D.; Burghardt, I.; Sommerfeld, T.; Hynes, J. T. *J. Phys. Chem. A* **2003**, *107*, 11271–11291.
(107) Burghardt, I.; Laage, D.; Hynes, J. T. *J. Phys. Chem. A* **2003**, *107*, 11292–11306.
(108) VandeVondele, J.; Mohamed, F.; Krack, M.; Hutter, J.; Sprik, M.; Parrinello, M. *J. Chem. Phys.* **2005**, *122*, 014515.
(109) Harder, E.; Eaves, J. D.; Tokmakoff, A.; Berne, B. J. *Proc. Natl. Acad. Sci. U.S.A.* **2005**, *102*, 11611–11616.
(110) Wallqvist, A.; Berne, B. J. *J. Phys. Chem.* **1993**, *97*, 13841–13851.
(111) Madden, P.; Kivelson, D. *Adv. Chem. Phys.* **1984**, *56*, 467–566.
(112) Fecko, C. J.; Loparo, J. J.; Roberts, S. T.; Tokmakoff, A. *J. Chem. Phys.* **2005**, *122*, 054506.

JP805217U